Current Research in Neurobiology 6 (2024) 100126

Contents lists available at ScienceDirect

Current Research in Neurobiology

journal homepage: www.sciencedirect.com/journal/current-research-in-neurobiology

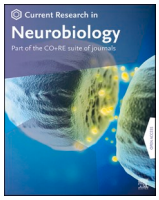

Decrease in phase slip rates and phase cone structures during seizure evolution and epileptogenic activities derived from microgrid ECoG data☆

Ceon Ramon [a,b,*], Alexander Doud [c], Mark D. Holmes [b]

[a] Department of Electrical & Computer Engineering, University of Washington, Seattle, WA, 98195, USA
[b] Regional Epilepsy Center, Harborview Medical Center, Department of Neurology, University of Washington, Seattle, WA, 98195, USA
[c] Providence Spokane Neuroscience Institute, 105 West 8th Avenue, Spokane, WA, 99204, USA

ARTICLE INFO

Keywords:
Phase slips
Microgrid EEG
Seizure localization
EEG phase cones
Phase transitions
EEG time series analysis

ABSTRACT

Sudden phase changes are related to cortical phase transitions, which likely change in frequency and spatial distribution as epileptogenic activity evolves. A 100 s long section of micro-ECoG data obtained before and during a seizure was selected and analyzed. In addition, nine other short-duration epileptic events were also examined. The data was collected at 420 Hz, imported into MATLAB, downsampled to 200 Hz, and filtered in the 1–50 Hz band. The Hilbert transform was applied to compute the analytic phase, which was then unwrapped, and detrended to look for sudden phase changes. The phase slip rate (counts/s) and its acceleration (counts/s^2) were computed with a stepping window of 1-s duration and with a step size of 5 ms. The analysis was performed for theta (3–7 Hz), alpha (7–12 Hz), and beta (12–30 Hz) bands. The phase slip rate on all electrodes in the theta band decreased while it increased for the alpha and beta bands during the seizure period. Similar patterns were observed for isolated epileptogenic events. Spatiotemporal contour plots of the phase slip rates were also constructed using a montage layout of 8 × 8 electrode positions. These plots exhibited dynamic and oscillatory formation of phase cone-like structures which were higher in the theta band and lower in the alpha and beta bands during the seizure period and epileptogenic events. These results indicate that the formation of phase cones might be an excellent biomarker to study the evolution of a seizure and also the cortical dynamics of isolated epileptogenic events.

1. Introduction

The formations of phase slips and phase cones are related to the coordinated activity of cortical neurons. It is theorized that the electrical activity of the cortex at any given time is very close to the state of criticality [Beggs and Timme, 2012] and any slight external or internal input could cause a state transition which will cause a group of neurons to fire in a coordinated fashion [Freeman et al., 2006a]. These state transitions produce sharp phase slips, also called phase jumps [Pikovsky et al., 2001], in the analysis of the EEG data by use of the Hilbert transforms. In coordination with similar phase slips on nearby electrodes form spatial patterns, called phase cones, and have been used to localize the epileptogenic sites from the seizure-free interictal EEG data [Ramon et al., 2013] and in the study of the cognitive behavior of the brain [Ruiz et al., 2010]. One can observe the amplitude and phase-modulated waves in theta (3–7 Hz) and alpha (7–12 Hz) bands with carrier frequencies in the beta (12–30 Hz) and low gamma (30–50 Hz) bands [Freeman et al., 2006a, Kozma and Freeman, 2017; Ruiz et al., 2010]. We have applied these similar techniques to study the dynamics of the phase slips and phase cones near to the seizure and epileptic activities from the micro-ECoG (μECoG) data of a subject which is something new and helps in better understanding of the dynamics of the seizure activity.

The data collected with implanted subdural microgrids provide a unique way to study the cortical electrical activity in humans and animals with high spatial (~1–5 mm) resolutions [Shokoueinejad et al., 2019; Wang et al., 2017; Kim et al., 2022]. These signals are called

Abbreviations: MAG, Magnification Factor; micro-ECoG or μECoG, micro-Electrocorticogram; PSR, Phase Slip Rate (counts/s); PSRs, Phase Slip Rates; PSA, Phase Slip Acceleration (counts/s^2). The differentiation (d/dt) of PSR is PSA.; RDM*, Relative Difference Measure.

☆ Some preliminary results were presented as a poster at the American Epilepsy Society Meeting, AES 2020; 4–8 Dec 2020. Abstract number: 72. Title: Phase oscillation frequency changes during evolution of an epileptic seizure: evidence from microgrid ECoG data.

* Corresponding author.
E-mail addresses: ceon@uw.edu (C. Ramon), Alexander.Doud@providence.org (A. Doud), mdholmes@uw.edu (M.D. Holmes).

https://doi.org/10.1016/j.crneur.2024.100126
Received 18 May 2023; Received in revised form 25 December 2023; Accepted 3 February 2024
Available online 19 February 2024

micro-electrocorticograms (micro-ECoG or μECoG) and have been used in several studies. In particular, an 8 × 8 microgrid of 3-mm interelectrode spacing has been used to study finger movements [Kuo et al., 2019, 2023]. Similarly, an 8 × 8 microgrid of 1.25 mm interelectrode spacing has been used to study the cortical phase slips during awake and sleep states [Freeman et al., 2006a, 2006b] and also in the different behavioral states of the brain, such as reading, telephone conversations, looking at photographs, etc. [Panagiotides et al., 2011]. This is a unique data set of one human subject collected at the University of Washington with a 1.25 mm spacing microgrid [Freeman et al., 2006a, 2006b]. The data collected with microgrids provide a better spatial resolution as compared with subdural grid or strip electrodes to study the oscillatory patterns of the cortical brain dynamics [Kleen et al., 2021; Seymour et al., 2017; Wang et al., 2017]. In particular, high resolution (1–1.25 mm) microgrids are very close to the size of cortical columns (~1.0 mm) and can pick up the local field potentials at mesoscopic scales in the brain [Pizarro et al., 2017] which, as shown, also helps in better control of finger movements [Kuo et al., 2019, 2023].

The description of the μECoG data set used in this study and the procedures to compute phase slips are given below in the Methods section. In the Results section, a detailed spatiotemporal analysis of the phase slip rates (PSR) and phase slip accelerations (PCA) during the seizure activity is given. Similar analyses for isolated epileptic events are also given. A critical analysis of our methods, results, and limitations of our study are included in the Discussion section.

2. Methods

2.1. μECoG data

We studied a 34-year-old woman with refractory focal impaired awareness seizures who underwent standard intracranial subdural strip electrode recordings to establish the localization of seizure onset. These subdural strip electrodes were placed over lateral and basal-temporal regions for preoperative evaluations prior to surgical intervention [Panagiotides et al., 2011]. In addition, after receiving IRB approval and with informed consent, a 1 × 1 cm, 8 × 8 contact microgrid with 1.25 mm interelectrode separation was applied to the surface of the right inferior temporal gyrus, near the location of the seizure-onset zone. The data were collected at the regional Epilepsy Center, Harborview Medical Center, University of Washington in Seattle. The subject underwent surgery and was free from seizures after the surgery and returned to normal life.

Electrographic data was recorded for eight days, with simultaneous video [Freeman et al., 2006a, 2006b; Panagiotides et al., 2011]. During these eight days, several epileptogenic and seizure related events were observed. The observed seizures were motor and non-motor related events. From these, we found eight data sets with good quality epileptogenic events and one long duration (~100 s) data set with seizure activity. These were free from motion artifacts and were selected for phase slip analysis. During the long-duration seizure, the subject did have progressive cognitive changes that included slowed thinking, increased anxiety, confusion, etc., but no motor-related symptoms. The first electrographic changes at the beginning of the seizure preceded the first clinical signs of the seizure by approximately 10 seconds.

In addition, for a comparative analysis, we used interictal data which was at least 2 h away from any seizure and epileptogenic activity. A 97 s long duration data was randomly selected for interictal phase slip computations and these results were compared with the ones derived from the seizure data.

Refer to Fig. 1 for details of the microgrid location and Fig. 2 for an example of the μECoG data. The electrode numbers are marked in the image coordinate system, i.e., the first pixel at the top left. This is also similar to the row and column numbering for a matrix. This is different from the (x, y) Cartesian coordinate system for plotting the data where the origin is at the bottom left, x increases from left to right and y increases from bottom to top. In Fig. 2, the first electrode #1 is at the top left and the last electrode #64 is at the bottom right. The electrode positions in the 8 × 8 grid system are also included. As an example, electrode #1 is at the grid position of (1, 1), #8 at the grid position of (1, 8), #57 at the grid position of (8, 1), and the electrode #64 at the grid position of (8, 8), respectively.

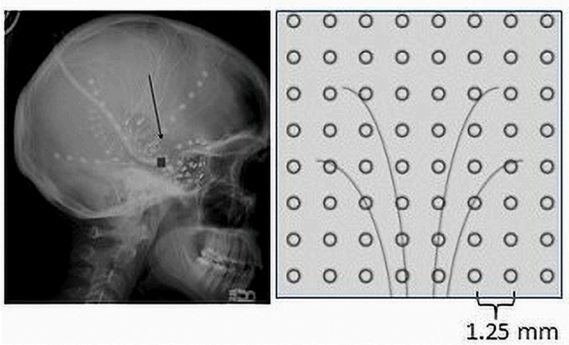

Fig. 1. (Left) X-ray of the skull showing the location of the microgrid with an arrow, (right) a schematic layout of the 8 × 8 micro-electrode grid with an interelectrode separation of 1.25 mm.

2.2. Phase slip extraction

The data was collected at 420 Hz, i.e., 420 samples/s, imported into MATLAB, down-sampled to 200 Hz, and filtered in the appropriate band. For example, filtered in 3–7 Hz for computing PSR and PSA in the theta band. The Hilbert transform was applied to compute the analytic phase, which was then unwrapped, and detrended to look for sudden episodic phase changes on multiple electrodes at the same time. Fig. 3 gives a pictorial representation of these mathematical procedures. The top plot is the 5-s μECoG data from one of the microelectrodes.

The Hilbert transform was applied to the μECoG data, and the phase was extracted. It comes out as a sawtooth pattern, not shown in Fig. 3, and it was unwrapped to give an approximately linearly increasing phase with time as shown in the second plot from the top. It shows episodic phase shifts marked by the sudden jumps in the unwrapped phase. These could show up on a few or on all 64 electrodes of the microgrid. Refer to Fig. 4 where the left plot shows the episodic phase shifts for all 64 electrodes and the right plot gives a detailed view of nearby four electrodes numbered as 27, 28, 29, and 30.

Now coming back to Fig. 3 again, the third plot from the top is for the phase frequencies. These were obtained by taking the derivative of the unwrapped phase which will be in the units of rad/sec. Dividing this by 2π gives us the phase frequency in cycles/s or Hz. There are sharp positive and negative peaks which are called phase slips that arise due to the coordinated activity of cortical neurons. However, the application of the Hilbert transform to EEG data will also generate these phase slips from random noise activity. To separate from the random noise activity, one needs to incorporate the biological and electrophysiological information regarding the firing of neurons [Freeman et al., 2006a; Ramon and Holmes, 2015, 2020; Ramon et al., 2018, 2023; Ruiz et al., 2010]. These include: (1) phase slip frequency is within a given temporal band, e.g., 7–12 Hz for the alpha band, (2) sign of the positive or negative peaks did not change for at least two consecutive time steps, (3) the magnitude of the two consecutive peaks was within the mean±2σ of the two peaks, and (4) episodic phase shifts of similar shape and size were observed on the nearby eight or more electrodes surrounding the particular electrode in the study and were within the range of conduction velocities of cortical axons, 1–10 m/s [Budd and Kisvárday, 2012; Swadlow and Waxman, 2012]. Application of these criteria will significantly reduce the counting of phase slips due to random noise.

The phase slip rate (PSR) in counts/s was computed with a stepping

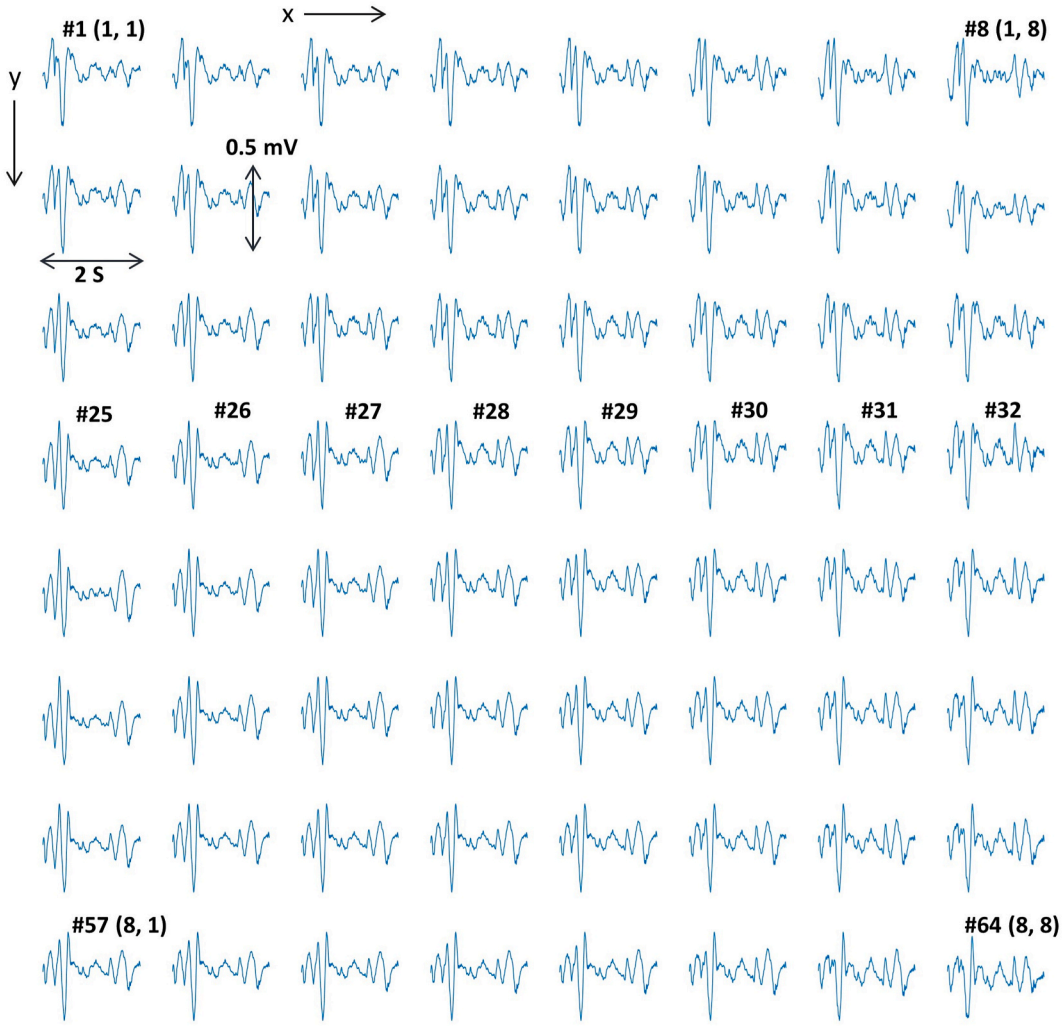

Fig. 2. An example of the μECoG data that includes some epileptic activity. A few electrode numbers are also marked for reference.

window of 1 s and with a step size of 5 ms which is based on the sampling rate of 200 Hz of the μECoG data. An example of the PSR and its acceleration is given in the fourth and fifth plots, respectively, from the top. The PSR tells us how fast the coordinated activity of neurons is changing with time which is dependent on the number of neurons taking part in the formation of episodic phase shifts. The change in the PSR is given by its acceleration which can be obtained either by differentiating the PSR or from the second derivative of the unwrapped phase. The acceleration tells us how fast the PSR is changing which could be related to the change in the rate at which the population of neurons is taking part in the formation of stable phase slips.

The first and second order differencing of time series data is very common in financial forecasting [Hyndman and Athanasopoulos, 2018] and also in the field of biomedical research [Brandenburg, 2019; Lara-Benítez et al., 2021]. However, its application to EEG data to analyze self-organized criticality and the phase reset is relatively new [Thatcher et al., 2009, 2014] and this could also be applied to study the behavior of phase slips during epileptogenic events. The first and second order differencing of a time series, $y(t)$, is related to first and second order derivatives (dy/dt and d^2y/dt^2) by the digitization interval, dt. The first-order differencing or derivative removes the linear trends in a given time series data. The second order differencing or derivative gives the curvature of the time series at a given point in time [Ravishankar, 1994]. If the curvature is zero, i.e., a flat horizontal line, the PSR will be increasing (or decreasing) linearly at a constant rate. If it is not flat, then the change in the PSR will be nonlinear.

The analysis was performed for theta (3–7 Hz), alpha (7–12 Hz), and beta (12–30 Hz) bands. Spatiotemporal contour plots of the phase change rate with 5 ms intervals were constructed using a montage layout of 8 × 8 electrode positions.

2.3. Phase slips from random data

The above analysis was also performed on the randomized μECoG data, and it was found that phase slips were zero in all the bands. This shows that our reported results are from the biological processes that give rise to the coordinated activity of cortical neurons which are above the random noise.

2.4. Statistical and comparative analysis

We used the Student's t-test and/or Kolmogorov–Smirnov test, also called, the K–S test or KS test to compare the similarities or differences between the means of two variables. The ANOVA analysis was performed to compare the means of more than two variables. The K–S test can be performed on two data vectors, x_1, and x_2, using a MATLAB function, kstest2 (x_1, x_2). As an example, x_1 and x_2 could be the phase slip rates in theta and alpha bands, respectively. The test is performed on the cumulative distribution functions, $F(x_1)$ and $F(x_2)$ of the data vectors, x_1 and x_2, respectively. The null hypothesis is that the two distributions are the same. If the null hypothesis is rejected, that would mean that the two distributions are different.

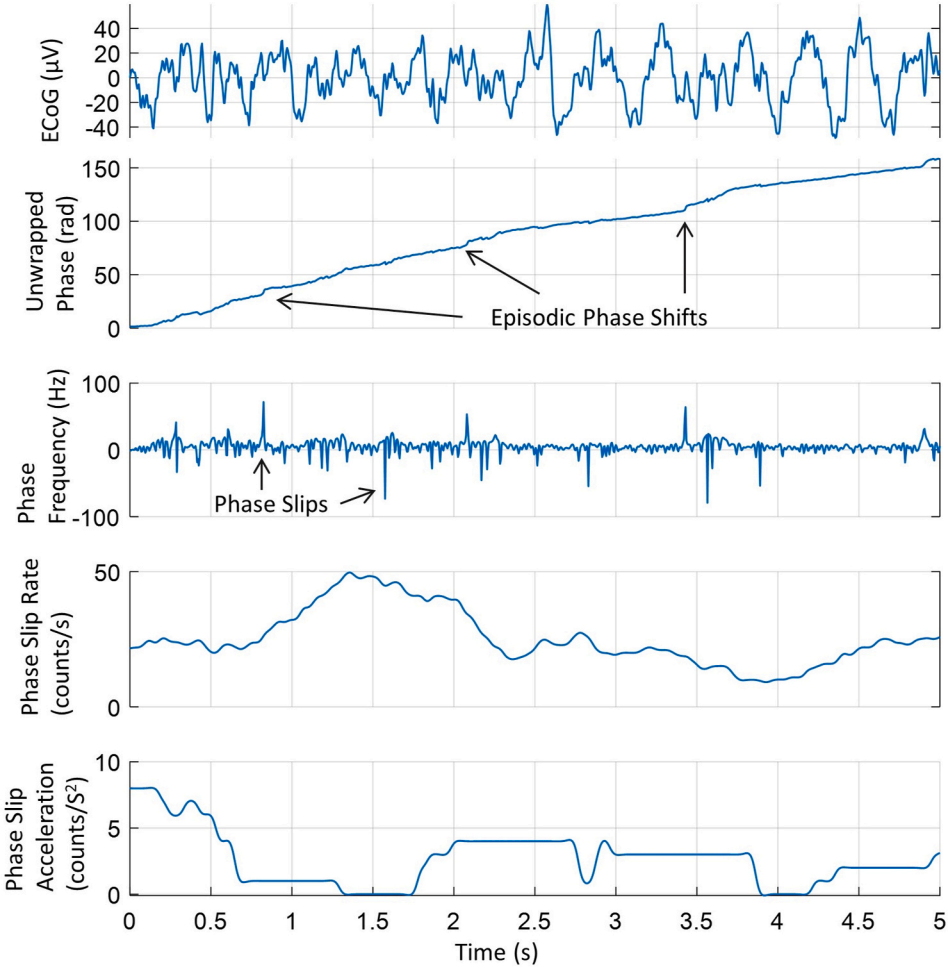

Fig. 3. A pictorial representation of phase slip extraction. (Top) A 5-s μECoG trace from one of the microgrid electrodes; (second from the top) unwrapped phase of the μECoG data; (third from the top) phase frequencies in Hz obtained after taking the derivative of the unwrapped phase and dividing by 2π; (fourth from the top) phase slip rate in counts/s; (bottom) acceleration of the phase slips in counts/s^2.

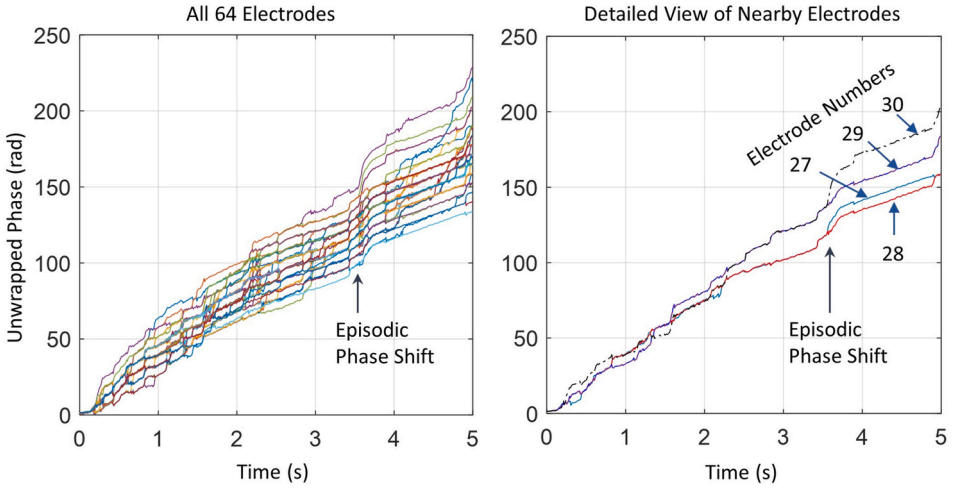

Fig. 4. (Left) Unwrapped phase of all 64 electrodes, (right) unwrapped phase of four adjacent electrodes numbered 27, 28, 29, and 30.

Z-score analysis was also performed to check for the differences in the normalized values of phase slip rates. It is difficult to perform a Student's t-test or ANOVA analysis on Z-scores to check if two distributions are the same or different because the data is already normalized to the mean ($\mu = 0.0$) values. However, this can be achieved with the K–S test.

We used quantitative indices to compare the spatial profiles of baseline values with the epileptic event values. This was done with the Relative Difference Measure (*RDM**) and magnification factor (*MAG*) [Meijs et al., 1989; Ramon et al., 2014; Schimpf et al., 2002]. It is a very

common technique to quantify the differences between two spatial plots. The *RDM** is defined as:

$$RMD^{*} = \sqrt{\sum_{j=1}^{m}\left[\frac{Z_k^{RM}}{\sqrt{\sum_{k=1}^{m}\left(Z_k^{RM}\right)^2}} - \frac{Z_k^{TM}}{\sqrt{\sum_{k=1}^{m}\left(Z_k^{TM}\right)^2}}\right]^2} \quad (1)$$

where index, $j = 1{:}m$, runs over all 64 microgrid electrodes, Z_k^{RM} and Z_k^{TM} are the RMS values of the phase slips (or PSR) at the kth electrode for the reference measurements (RM) and the test measurements (TM), respectively. The magnification factor is defined as:

$$\mathrm{MAG} = \frac{\sqrt{\sum_{k=1}^{m}\left(Z_k^{TM}\right)^2}}{\sqrt{\sum_{k=1}^{m}\left(Z_k^{RM}\right)^2}} \quad (2)$$

The *RDM** is a measure of the difference in spatial profiles of two data sets and *MAG* is a measure of differences in the magnitude of the two data sets. If two data sets are the same, *RDM** will be zero and *MAG* will be unity. The degree of differences is quantified with higher values of *RDM** in the range of 0.0–1.0. The maximum value of *RDM** is 1.0 if the test measurements are zero. The variation in the value of *MAG* from unity will quantify the differences in the magnitude of the two data sets. Values of *MAG* greater than 1.0 would mean that the test measurements (TM) are higher in magnitude as compared with the reference measurements (RM). And the reverse is true if *MAG* is less than 1.0.

For a comparative analysis, an epileptic event could be one or few seconds long and the baseline could be similarly one or few seconds long data before the epileptic event. The RMS (Root Mean Square) values of phase slips for baseline and the epileptic event for all 64 electrodes were computed. Phase slips are both positive and negative (Fig. 3, second plot from the top), therefore, RMS values are the best to use. These values were then used to quantify the spatial differences over all sixty-four electrode values between the baseline (reference measurements, RM) and the nearby epileptic event (test measurements, TM).

3. Results

3.1. Analysis of seizure data

3.1.1. Seizure data plots

One of the data sets had a prolonged seizure activity of about 100 s duration. In our data set, it is marked as seizure #9. Analysis of this data set is given in Fig. 5.

It shows (top plot in Fig. 5) one trace of approximately 100 s long μECoG data on electrode #28. Intermittent epileptic activity is present from the beginning to the end of the μECoG trace. The seizure onset time is from 0.0 s. In addition, there is a prominent epileptic event around 9.5 s and a prolonged increasing amplitude μECoG seizure activity during the period of 40–97 s. Similar epileptic activity patterns were observed on all sixty-four electrodes of the microgrid. A distinctive pattern of seizure activity is recognizable between the period of 57–97 s. The evolution of seizure activity is present during the period of 40–57 s. The bottom three plots in Fig. 5 are for phase slips in theta, alpha, and beta bands.

The PSR in the theta band goes down during the seizure activity (57–97 s) with a concave temporal shape during this period. In contrast, the PSR in alpha and beta bands goes up with a convex shape during this period. In addition, low-frequency oscillations are riding on the broad concave or convex shapes of PSRs.

A one-way ANOVA analysis was performed on the PSR values of electrode #28. It was found that the PSR for theta, alpha, and beta bands are significantly ($p < 0.01$) different from each other. A similar analysis was performed for other remaining electrodes and the PSR values for all electrodes were found to be significantly ($p < 0.01$) different from each other.

3.1.2. Z-score analysis of seizure data

A Z-score analysis of PSRs for electrode #28 was also performed. These are plotted in Fig. 6. The temporal changes in the Z-scores over the 0–97 s period are given in Fig. 6(A). The cumulative distribution functions of Z-scores are given in Fig. 6(B). Here *F(x)* is the cumulative distribution of *x* where *x* is one of the Z-scores. As an example, *x* could be

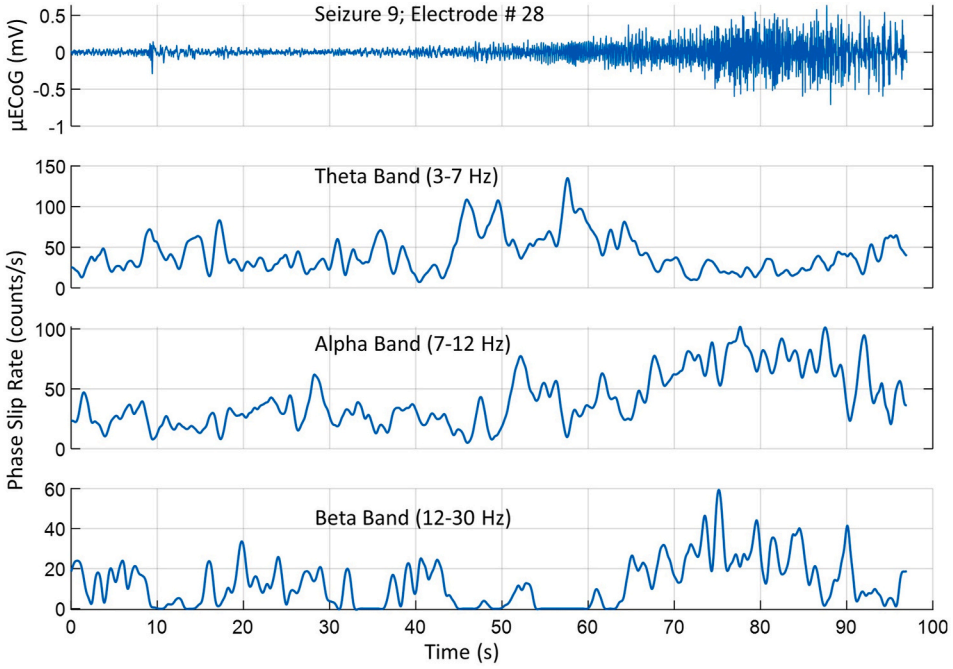

Fig. 5. Phase slip analysis of the seizure activity. (Top) μECoG activity on electrode #28. It shows a prominent epileptic event around 9.5 s and sustained seizure activity during the period of 40–97 s (Three bottom plots) The phase slip rates in theta, alpha, and beta bands, respectively. Notice during the 60–90 s period, the theta band activity goes down while alpha and beta band activities go up.

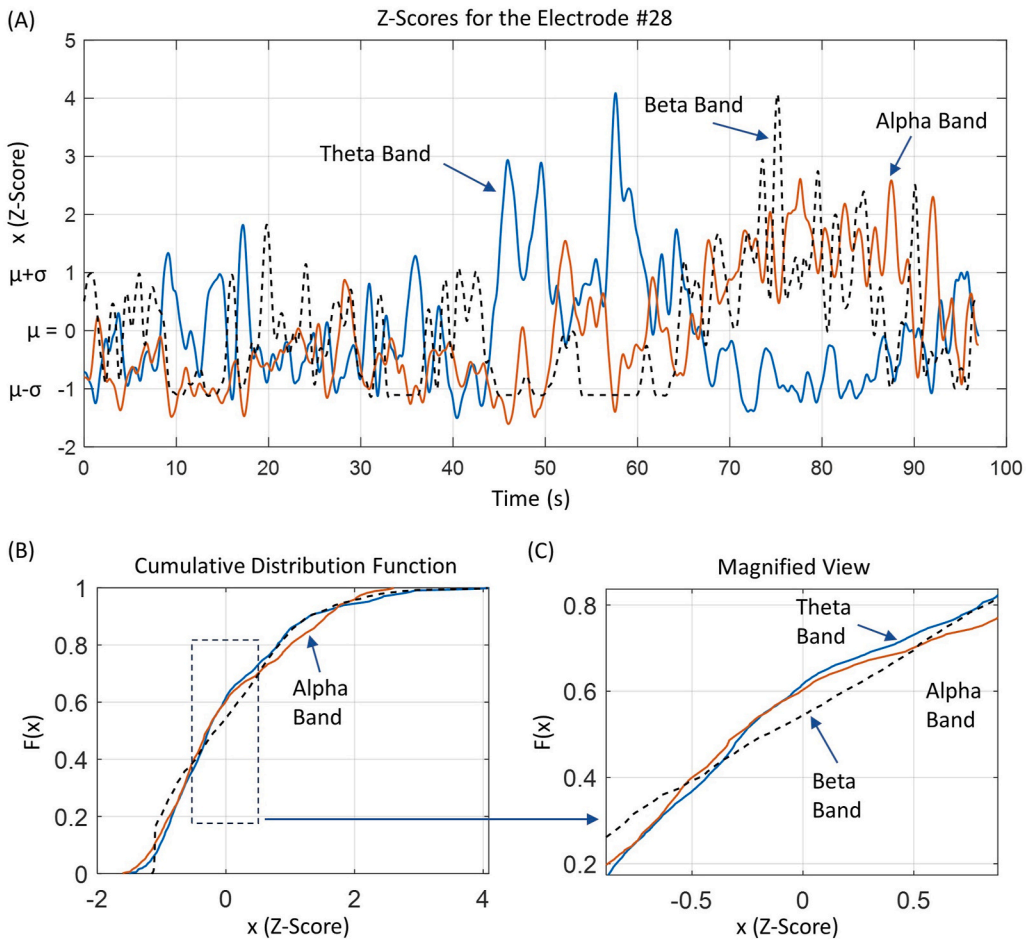

Fig. 6. (A) Z-scores of phase slip rates in theta, alpha, and beta bands for electrode #28, (B) cumulative distribution functions, *F(x)* of Z-scores called as *x*, and (C) expanded view of a small segment of *F(x)*.

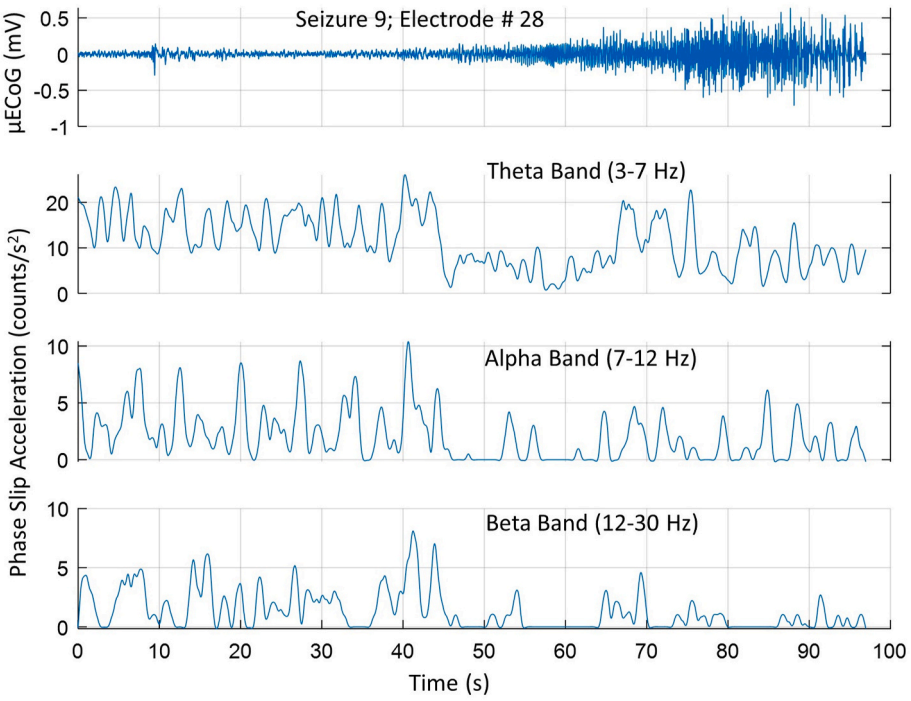

Fig. 7. Acceleration of the phase slip rate on electrode #28 in all three bands. (Top) EEG trace, (bottom three plots) acceleration in the theta, alpha, and beta bands.

the Z-score in the theta, alpha, or beta band. An expanded view of a small segment of $F(x)$ is given in Fig. 6(C).

The Z-scores for each band are normalized to a value of zero mean, $\mu = 0.0$. Most Z-scores are within the limits of $\mu \pm 2\sigma$, where σ is the standard deviation. This covers 95.44% of all the Z-score values. However, some remaining (<4.56%) values are in the higher range ($>\mu \pm 2\sigma$). We performed this K–S test on the Z-score values given in Fig. 6(A) for theta, alpha, and beta bands. A combination of theta and alpha Z-scores, or theta and beta Z-scores, or alpha and beta Z-scores were used for the K–S test. The null hypothesis was rejected for all three cases, suggesting that Z-scores for electrode #28 shown in Fig. 6(A) are different from each other ($p < 0.01$). A similar analysis was performed for Z scores of PSR values for other electrodes and the outcome was similar. This shows that statistical analysis results are the same whether performed on the PSR values or on Z-scores of PSR values.

3.1.3. Analysis of phase slip acceleration of seizure data

The accelerations of phase slips for all three bands are given in Fig. 7. Between zero and 40 s, the activity is mostly the low level seizure activity and after that, during 40–97 s it is the sustained seizure activity. During the period of 40–45 s, the acceleration in the theta band slightly rises and then falls rapidly to zero. This pattern is also present in the alpha and beta bands with well-defined epileptic events at 41 and 44 s. After that, low-level acceleration activity in the theta band continues during the 50–57 s period with overriding small oscillations. This is also reflected in the oscillatory changes in the PSR between 100 and 140 counts/s (Fig. 5) in the theta band. After that, the PSR (Fig. 5) in the theta band has a negative parabolic shape with superimposed oscillations. Related to this, the acceleration (Fig. 7) has varying oscillations in the range of 0–22 counts/s^2. In contrast, the PSA in the beta band is less in magnitude (0–10 counts/s^2) with intermittent sharp well-defined peaks. A similar pattern is present for the beta band (bottom plot in Fig. 7) with the magnitude of the peaks in the range of zero to 4 counts/s^2 during the period of 50–97 s.

The coordinated phase slip activity, i.e., PSR and PSA, on all 64 electrodes for the 0–97 s period is given in Fig. 8. This coordinated phase activity on all electrodes has also been observed before during the sleep and awake states [Freeman et al., 2006a, 2006b] which is similar to what we are seeing in the seizure activity. A pattern to note is that during the early seizure period (~0–50 s), the PSR is lower on all electrodes as compared with the seizure activity during the 50–97 s period. In the theta band, the PSR activity is high (~200 counts/s) during the 43–60 s period, then it slowly declines during the 57–80 s period and increases slightly during the 80–97 s period. It is slightly different in alpha and beta bands. The alpha band activity in 60–97 s duration has a convex shape on all electrodes which peaks around 75 s. Overall there is phase coordination on all electrodes at a given time point. A similar pattern is present in the beta band activity within the magnitude range of 0–60 counts/s.

In relation to the PSR, the acceleration on all electrodes is also given in Fig. 8. An interesting feature to note is that during the initial 0–40 s period, all three bands have high amplitude and exhibit an oscillatory pattern in space, i.e., over 64 electrodes, and in time. During the next period, 45–67 s, the acceleration is low in magnitude on all electrodes in

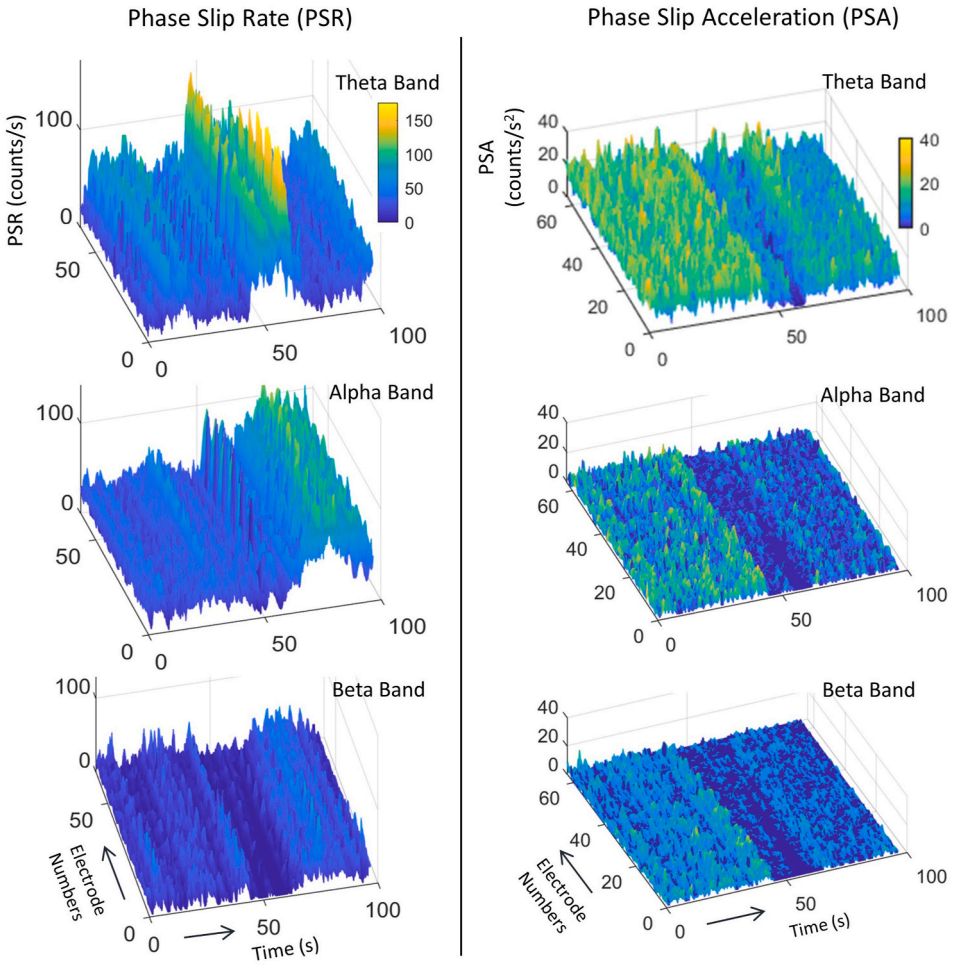

Fig. 8. Coordinated activity of phase slip rates (PSR) and phase slip acceleration (PSA) in theta, alpha, and beta bands on all 64 electrodes during the time period of zero to 97 s.

all three bands. After that, it slightly goes up and has an oscillatory pattern during the seizure period of 67–97 s.

3.1.4. Spatial profiles of phase cones

The spatial profiles of PSR provide a unique view to observe the formation and dissipation of phase cone structures which have been suggested and observed before in the rabbit data [Kozma and Freeman, 2017; Myers et al., 2014], and also in human microgrid data during awake and sleep states [Freeman et al., 2006b]. We are seeing similar spatial patterns during the seizure period also. It will be difficult to show these patterns over the complete 100 s duration of the seizure data. However, in short duration of few seconds it is feasible and it is shown in Fig. 9. This duration was chosen to see a complete waxing and waning cycle of a phase cone formation. The *x and y* coordinates are marked in the top right plot. The *z-axis* is the PSR values which is also color coded. Refer to the bottom right plot for the color scale for PSR.

The PSR values are larger in the theta band as compared with the alpha and beta bands. In the theta band one can see the formation of a phase cone pattern in the rear starting from 43 s which maximizes at 46 s, and then begins to subside till 48 s. After that formation of a new pattern begins to emerge at 49 s. In the alpha band, the magnitudes are smaller than the theta band, but, one can still see formation of a phase cone in the frontal area which peaks around 45 s and then slowly begins to disperse in the following frames. For the beta band, there is formation of a phase cone in frontal area from 40 s onwards and becomes predominant in the 44 s time-frame. After that it begins to fade and disperse in the rear area between 46 and 48 s time-frames. In the beta band, there is formation of phase cone in the frontal area starting at 42 s which peaks around 44 s, and then begin to diminish and shift slightly toward the left frontal area. Also, one can see the formation of a new phase cone in the

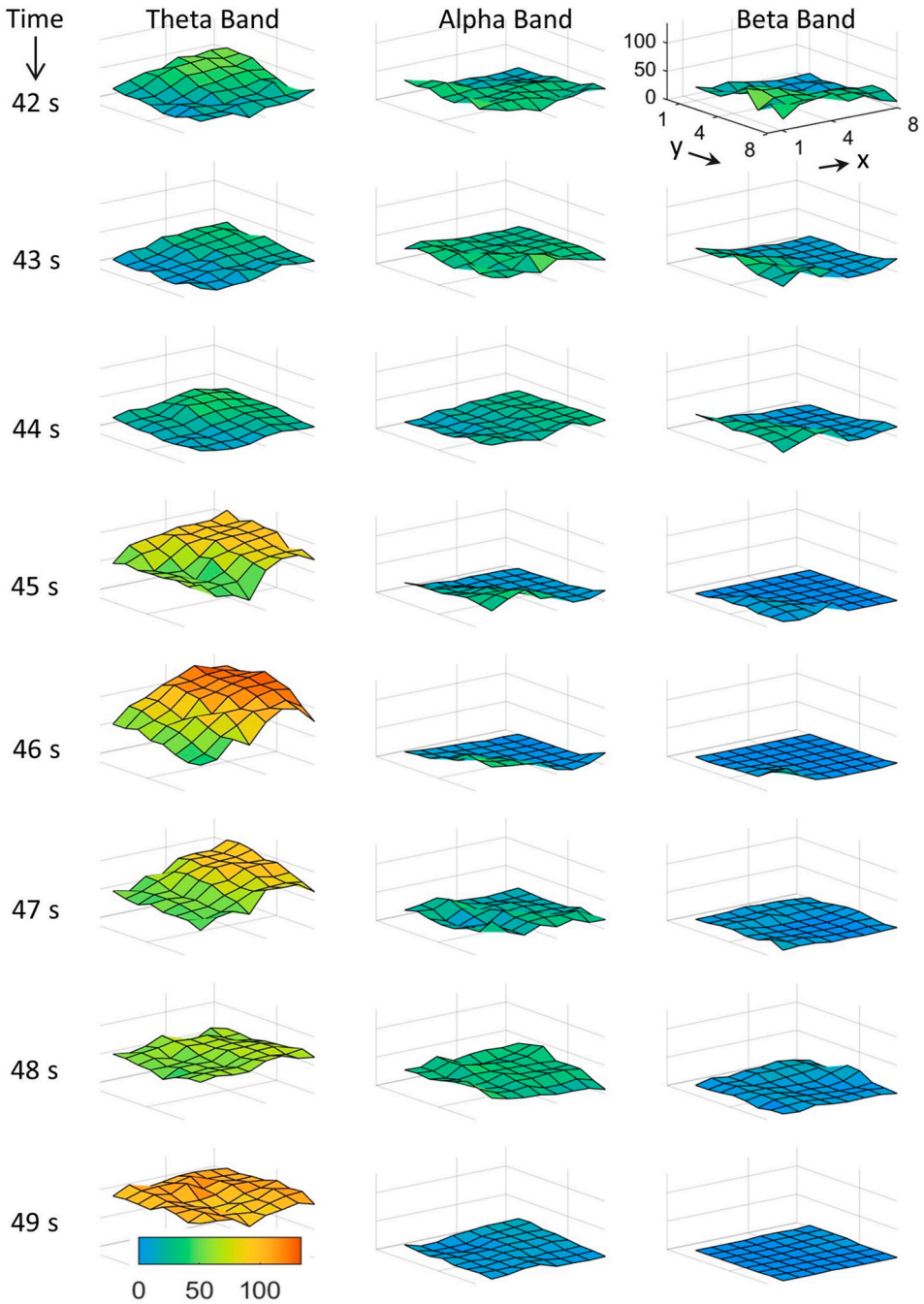

Fig. 9. Spatial profiles of phase slip rates during the seizure period of 42–49 s.

48 s frame in the rear area.

3.1.5. Comparison of PSR and PSA during interictal and seizure periods

A comparative analysis of the PSR and PSA during the interictal and seizure periods was performed. A 97 s long duration of the interictal data was randomly selected which was free from any epileptogenic activity [Freeman et al., 2006a, 2006b; Panagiotides et al., 2011]. This duration is similar to the duration of the seizure #9 data. The PSR and PSA were computed for this interictal data and then averaged over the 97 s period. Similarly, PSR and PSA for the seizure were averaged over the 97 s duration. This was done for each electrode. These averaged quantities for the alpha band are given in Fig. 10. The top plot is for the averaged PSR (counts/s) in the alpha band for the interictal and the seizure data, and the bottom plot is for the averaged PSA (counts/s^2). An interesting thing to note is that the averaged PSR for each electrode is higher for the interictal data as compared with the seizure data. While the reverse is observed for the averaged PSA. The reason could be that the synchronization between the nearby neurons is disrupted during the prolonged seizure activity. More about this is explored in the discussion section.

The similarities and/or differences in values between the interictal and seizure PSR were determined with a paired Student's t-test and also with the K–S test. With both methods, it was found that PSR values in the alpha band (Fig. 10) band were significantly ($p < 0.01$) different. Similarly, it was found that PSA values for the interictal and seizure were also significantly ($p < 0.01$) different. This analysis was repeated for PSR and PSA values in the theta and beta bands and the results were similar to what was observed in the alpha band.

3.2. Analysis of an isolated epileptic event

As shown in Fig. 5, there is a well-defined epileptic event between 9 and 10 s where one can perform a detailed analysis. For this purpose for a short duration of 5–10 s, the PSR and the acceleration (PSA) for electrode #28 in all three bands are plotted in Fig. 11. For a comparative analysis, we will call 8–9 s as the baseline period and 9–10 s as the epileptic event period. Both are of the same duration of 1.0 s.

In the theta band, the PSR rises approximately in a linear fashion from 27 to 70 counts/s during the baseline period and decreases from 70 to 58 during the epileptic event. In contrast, the PSR in the alpha and beta bands goes down during the epileptic event. For the alpha band, the PSR ranges from 40 to 20 counts/s during the baseline (8–9 s) and between 20 and 7 counts/s during the epileptic event (9–10 s). The PSR in the alpha band has a linear decline from 8.3 to 9.5 s and then begins to rise gradually. The beta band PSR, in contrast, declines during the baseline period and then afterward remains flat, close to the zero value, during the epileptic event period of 9–10 s. So for this particular electrode #28, the changes in PSR for the theta band are substantial while the changes in the alpha and beta bands were relatively small.

The acceleration goes down in all three bands during this epileptic event period. The acceleration in the theta band during the epileptic event period (9–10 s) is about 10 counts/s^2 while in alpha and beta bands is about 1–3 counts/s^2 which is very low as compared with the theta band activity.

The spatial profiles of phase slip rates before and during (8–9.75 s) the epileptic event are given in Fig. 12. The profiles are plotted on a montage layout of an 8 × 8 electrode grid. The *x* and *y* coordinates are shown in the top plot of the beta band. The first electrode will be at the front left corner ($x = 1, y = 1$) and electrode #64 will be at coordinates ($x = 8, y = 8$) at the right back corner of the plot. The electrode numbers increase from left to right on the *x-axis* and front to back on *the y-axis*. This is different from the image coordinate system used in Fig. 2 to show the μECoG data on all sixty-four electrodes in the 8 × 8 grid.

There are spatial formations of phase cone structures in all three bands which change with time. The magnitude scale is the same for all these plots. In the theta band, there is an increase in the magnitude of phase cones as one moves from 8 s toward 9.25 s time frames and then it begins to decrease after that. Looking at the plot at 9.25 s for the theta band, one can see a distinct peak at the back on the fourth electrode, i.e., electrode position (4, 8). A negative peak is toward the right front area in the 8.5 s frame which is overshadowed by other peaks in the later time frames. The behavior of spatial profiles in the alpha band is significantly different from the theta band. There are distinct formations of two different phase cones in the 8 s frame (top plot, alpha band) which slowly diminishes till the 9 s frame. During 9–9.75 s the phase cones have disappeared and there is some newer activity at the right back edge of the frames. Similar spatial patterns are visible for the beta band activity. This behavior of spatial phase cones in the alpha and beta bands has been suggested previously [Freeman et al., 2006a, 2006b]. It was suggested that, in general, the spatial structure of phase cones will be well-defined and stronger before an event and will slowly disintegrate near and during an event. An event could be a cognitive event or an epileptic event that, in theory, could disrupt the coordinated phase

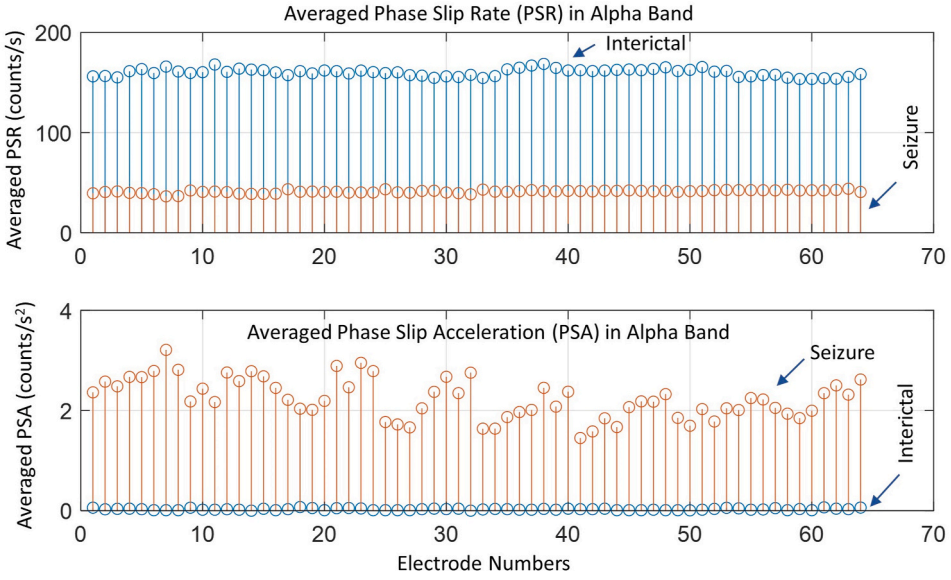

Fig. 10. (Top) Stem plot of averaged phase slip rates (counts/s) in the alpha band during interictal and seizure #9 event for all electrodes, (bottom) stem plot of the averaged phase slip accelerations (counts/s2) for all electrodes. Notice that PSR is higher for the interictal data while the PSA is higher for the seizure data.

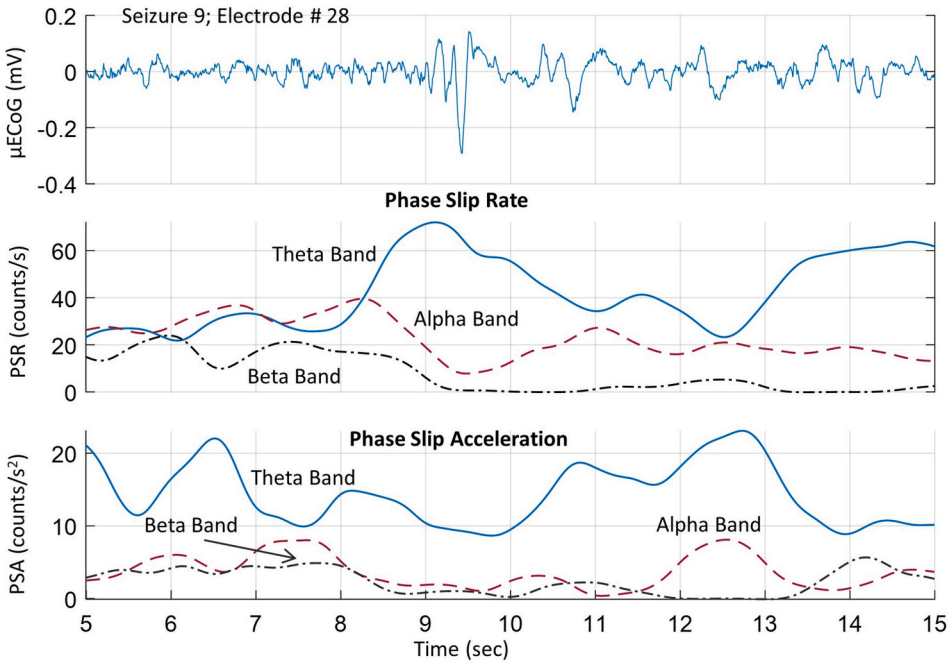

Fig. 11. Coordinated activity of phase slip rate and the phase slip acceleration in theta, alpha, and beta bands for an isolated epileptic event during 9–10 s.

activity of cortical neurons.

A statistical analysis of the differences in spatial profiles during the baseline and epileptic event was performed using the Relative Difference Measure (*RDM**) and *MAG*, defined by equations (1) and (2). For this epileptic event, the *RDM** values for PSR in theta, alpha, and beta bands are: 0.1079, 0.5392, and 0.8162, respectively which are higher than zero and significantly different from each other. These values suggest that in the theta band, the RMS values of PSR during an epileptic event are about 11% (with round-off) higher as compared with the baseline. Similarly, these changes are about 54% and 82% respectively for the alpha and beta bands. The *MAG* values in the theta, alpha, and beta bands are: 1.0707, 0.5654, and 0.138, respectively. The differences between these *MAG* values are also significant. In summary, these values of *RDM** and *MAG* combined together reflect that the PSR of an epileptic event over the nearby baseline values are significantly different. An ANOVA analysis is given in the next section.

3.3. Analysis of other isolated epileptic events

Similar to the event shown in Fig. 11, we randomly selected nine other isolated epileptic events from the seizure data, and the *RMD** and *MAG* analyses were performed on them in theta, alpha, and beta bands. These values are given in Table 1. From the mean±std values of ten events in Table 1, one can infer that during an epileptic event, the changes in *RDM** are 15.7%, 42%, and 66.7 % in the theta, alpha, and beta bands, respectively. As stated earlier, $MAG = 1.0$ means that the two data sets are the same. For the theta band, the *MAG* is 1.07, suggesting that the epileptic event values are 7% higher than the baseline values. This is a very small change in the magnitude values. For the alpha band, the *MAG* is 0.89, suggesting that the epileptic event values are about 11% lower than the baseline. Similarly, in the beta band, the epileptic event values are 14% lower than the baseline values. A one-way ANOVA analysis with two groups was performed on the *RDM** and *MAG* values given in Table 1. One group was *RDM** and the other group was *MAG*. It was found that the values in the theta, alpha, and beta bands are significantly different from each other ($p < 0.01$).

4. Discussions

These results suggest that one can study the changes in phase slip rates, phase slip acceleration, and spatiotemporal phase cone formations before and during an epileptic seizure or an epileptic event, such as an epileptic spike. These phase slips are related to the cortical phase transitions and may be helpful biomarkers in the study of the evolution of seizures and suggest that even within small regions, such as 1 × 1 cm size of the brain tissue one can observe changes related to cortical phase transitions. We have shown these from the microgrid data of one subject only. However, such data sets are difficult to collect, but, it will be good to confirm these findings from data sets of a few other subjects. Even from one subject, we have uniformity of results for ten isolated epileptogenic events. This, in one way, confirms that our procedures and reported results are reliable. We and others have used similar mathematical procedures to look for cortical phase transitions from EEG and ECoG data sets [Kozma and Freeman, 2017; Ramon et al., 2013, 2018, 2023; Ruiz et al., 2010].

We have shown changes in phase slip rates and their accelerations during the evolution of a one-long seizure. In this respect, our results are limited because we were able to identify only one good gradually evolving artifact-free seizure. This certainly needs to be confirmed from the analysis of more data sets and we hope that some other research groups with similar data sets will take the lead on this. Further studies are also needed to better characterize these phenomena in the context of pharmacologic treatment of epilepsy and in the context of the larger brain network recordings with electrode arrays like stereo EEG, subdural grids, and microgrid recordings. In addition, the tools developed here for epileptogenic events can also be applied to the study of the coordinated phase-related activity of cortical neurons under different conditions, such as resting state or different cognitive states of the brain.

The phase slip acceleration was computed after second order differencing of the unwrapped phase which was obtained from EEG data using the Hilbert transform. The second order differencing of EEG time series data or its derived unwrapped phase is not a common procedure for the analysis of the EEG data. However, as mentioned earlier, it is a very common procedure in economic forecasting [Hyndman and Athanasopoulos, 2018]. It has been applied to study the phase resetting of the default mode networks and also for the self-organized criticality of brain

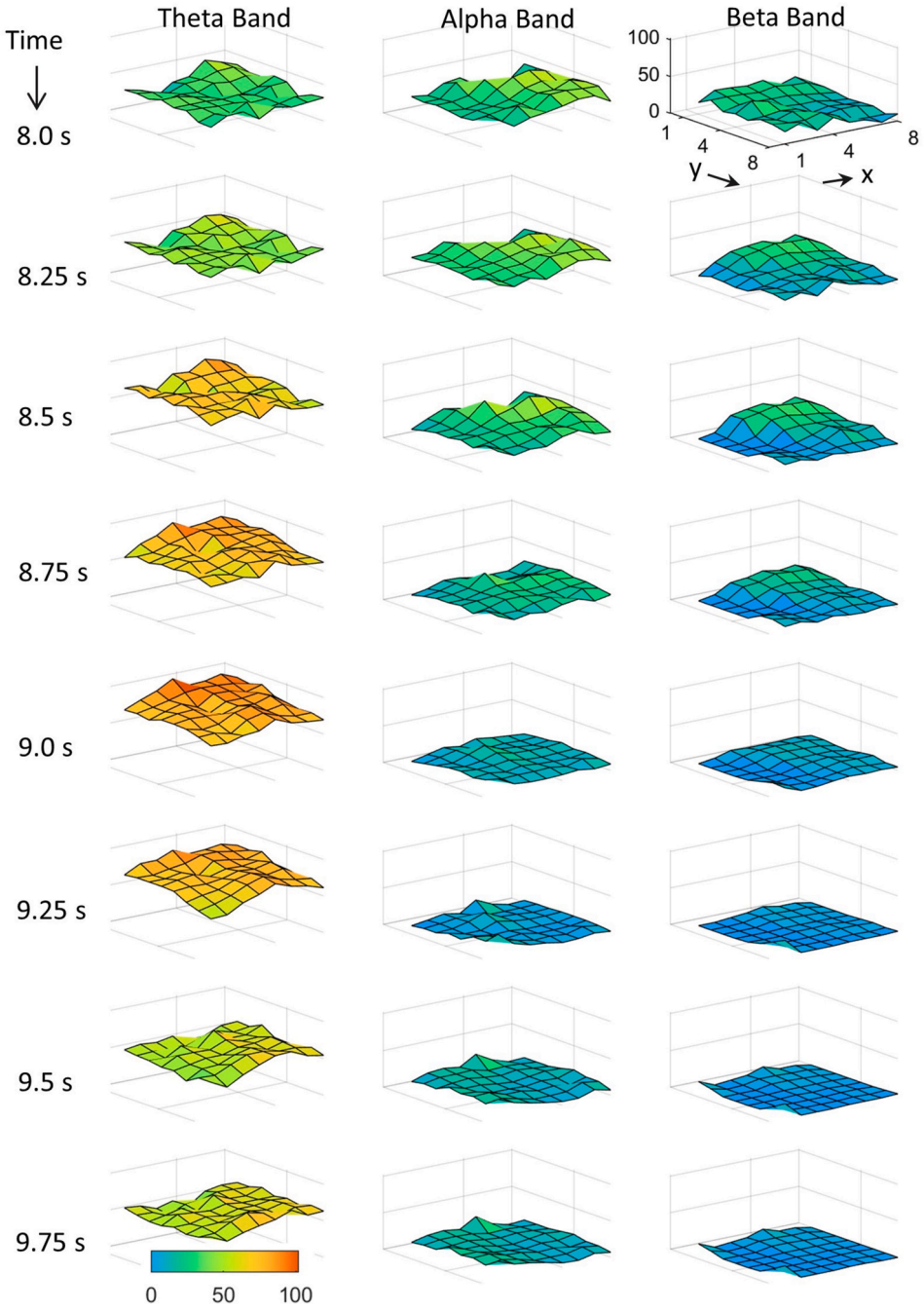

Fig. 12. Spatial profiles of phase slip rates during the 8.0–9.75 s period in theta, alpha, and beta bands. Notice spatial formations and dissolutions of phase cones in all three bands at different time points.

networks [Thatcher et al., 2009, 2014] which leads toward the cortical phase transitions due to internal or external stimuli [Freeman et al., 2003; Kozma and Freeman, 2017]. In this study, we have applied similar procedures to examine the phase slip acceleration during epileptic seizures. This is something new to our knowledge and opens a new way to examine how fast the cortical phase transitions change during a seizure or an epileptogenic event.

One thing to note is that the phase slips are not related to the amplitude of the electrical data, i.e., EEG, ECoG, or μECoG. These are, in contrast, related to small perturbations in the electrical data which on the application of the Hilbert transform give rise to a $\pm\pi$ phase shift at each perturbation [Ramon et al., 2023]. So even during the seizure, when the EEG amplitude becomes larger, it does not automatically increase the rate of formation of phase slips or phase cones. The PSR and PSA rather depend on the phase coordination of a group of neurons at mesoscopic (~0.5 mm) scales that give rise to the burst oscillations and the formation of small perturbations in the EEG data [Kozma and Freeman, 2017; Freeman and Quiroga, 2013]. An interesting feature was found that during the prolonged seizure activity, the PSR decreased in the theta band while increasing in the alpha and beta bands. Refer to Figs. 5–7. In addition, there are low-frequency (<1 Hz) oscillatory patterns overriding the profiles of phase slip rates and phase slip accelerations. Periodic slow waves have been observed in ictal and seizure EEG data [Kantzeli et al., 2021; Yasugi et al., 2018]. It is a possibility that these oscillations and behavior of PSR in different EEG bands might be related to slow changes in the local field potentials caused by groups of neurons joining and/or leaving the seizure activity [Wu et al., 2018]. This needs to be further investigated.

Table 1
Relative Difference Measure (*RDM**) and Magnification (*MAG*) factor analysis of ten epileptic events.

Event#	Theta (3–7 Hz) Band		Alpha (7–12 Hz) Band		Beta (12–30 Hz) Band	
	*RDM**	*MAG*	*RDM**	*MAG*	*RDM**	*MAG*
1	0.1079	1.0773	0.5392	0.5654	0.8162	0.1738
2	0.1804	0.7866	0.2802	1.0572	0.7068	1.9618
3	0.0895	1.0303	0.3869	1.2908	0.7575	0.8808
4	0.0930	1.0780	0.4580	0.4300	0.8540	0.2500
5	0.2191	1.1455	0.4768	0.6542	0.5739	0.5121
6	0.2347	1.2723	0.5114	0.3529	0.5878	0.3367
7	0.1612	1.2715	0.3120	0.9560	0.1312	0.5589
8	0.1580	1.0749	0.3340	0.8044	0.3439	0.7114
9	0.1588	0.9844	0.3549	1.3494	0.7685	1.0673
10	0.1689	0.9864	0.5465	1.4364	1.1288	2.1554
μ±std	0.16 ± 0.05	1.07 ± 0.14	0.42 ± 0.1	0.89 ± 0.39	0.67 ± 0.28	0.86 ± 0.69

ANOVA ($p < 0.01$).

A limitation of our study was that the analysis was performed at the sampling rate of 200 Hz, which was sufficient to find stable phase slips above the noise in the theta, alpha, and beta bands. However, it failed to produce any reliable results in the low gamma (30–50 Hz). The temporal profiles showed only intermittent activity in the low gamma band. A similar study was performed on the rabbit data, sampled at 500 Hz where they were able to see phase cone formations up to 40 Hz [Freeman and Barrie, 2000; Myers et al., 2014]. In another recent study, the phase slip formations during visual cognitive processes were examined with EEG data collected at a high sampling rate of 16.384 kHz [Ramon et al., 2023]. In this study, a high sampling rate helped in a detailed spatiotemporal analysis of phase slips in the theta alpha and low gamma bands. Thus, a higher sampling rate seems to help for better detection of cortical phase transitions and computations of associated phase slip rates in the low gamma band. Perhaps, based on previous studies [Ramon et al., 2013, 2018, 2020] a sampling rate of 1.0 kHz or higher might be better suited for cortical phase transition studies in the EEG frequency ranges of low (30–50 Hz) gamma, high (50–80 Hz) gamma, and ripple (80–250 Hz) bands.

There is a presence of slow (~0.1–7 Hz) wave oscillations and also there are differences in the spatiotemporal profiles of phase slip rates of theta alpha and beta bands. Similar slow-wave oscillations in delta and theta bands have also been observed in the phase-amplitude coupling derived from subdural grid recordings of epileptic patients [Hashimoto et al., 2021, 2022], in spatial phase cone patterns near epileptic spikes derived from 256 channel scalp EEG recordings [Ramon et al., 2018], and in the phase slip rates during visual object naming tasks in normal subjects [Ramon et al., 2023]. Most of these slow wave oscillations and related temporal variations in different EEG bands probably arise from the cortical rhythms in the brain which can be modeled by use of neural mass models in the normal and diseased states [Bhattacharya et al., 2011; Jansen and Rit, 1995; Jirsa et al., 2023; Pinotsis et al., 2012]. One can model these oscillations in small volumes of cortical tissue at mesoscopic scales (~0.5 mm) using simple neural mass models [Jansen and Rit, 1995]. This can be achieved by changing the values of connection weights between pyramidal neurons, excitatory interneurons, and inhibitory interneurons to model the cortical rhythms. For larger areas of the brain, one can use interconnected neural mass models [Bhattacharya et al., 2011; Jirsa et al., 2023] to simulate cortico-cortical and thalamocortical oscillations in normal and diseased states by changing the connection weights and the velocity of propagation on fiber pathways [Swadlow and Waxman, 2012]. One must go deeper into the physics of cortical electrodynamics for simulations of cortical phase transitions. As stated in the Introduction the electrical activity of the cortex is constantly in a metastable state and a slight input, internal or external, could cause a state transition which could be modeled as a dissipative many-body field theory problem [Capolupo et al., 2013; Freeman and Vitiello, 2006; Kozma and Freeman, 2017] or as neural avalanches [Beggs and Timme, 2012; Wang et al., 2023], or as mean-field models [Toker et al., 2022]. These models can predict the formation of low-frequency oscillations. A combination of these theoretical models and simulation methods might help to explain our observed results and we hope that some research groups can explore this further.

This μ-ECoG data was originally collected by Walter J. Freeman III and has been used to study changes in the phase differences during awake and sleep states, and during pre-ictal and seizure periods [Freeman et al., 2006a, 2006b]. From the same data, they studied spatial variations of the μ-ECoG potentials and found them to be significantly different under various behavioral states, such as reading, telephone conversations, looking at photographs, etc. [Panagiotides et al., 2011]. In any of these studies, phase slip rates or phase slip accelerations were not computed or studied. In this regard, the work reported here is relatively new and should be considered as a natural and logical extension of previous works of Freeman's group [Freeman et al., 2006a, 2006b]. We have recently published some protocols and related results on changes in PSR during visual object naming tasks [Ramon et al., 2023]. Similar protocols have been utilized here to compute PSRs from the μ-ECoG during prolonged seizure periods. To our knowledge, applying phase slip acceleration (PSA) techniques to seizure evolutions is relatively new. In the future, these might become additional routine biomarkers to analyze the EEG data of normal subjects and patients. This will help to map how fast the cortical phase transitions influence the brain's electrical activity.

The micro-seizures are observable in μ-ECoG data which are difficult to see in scalp EEG or subdural grid recordings [Stead et al., 2010; Sun et al., 2022]. Also, it has been suggested that an interelectrode spacing of 3.0 mm is needed for the extraction of cortical patterns from scalp EEGs [Ramon et al., 2009]. This criterion also applies to subdural grid recordings. Thus, in essence, microgrid recordings are the best choice to map microseizures. The PSR computed from the μ-ECoG data gives us a high-resolution picture of the formation and dissolution of spatial phase cones at the mesoscopic scale which is difficult to ascertain from scalp EEG or subdural grid recordings. Thus, PSR and PSA derived from μ-ECoG data are unique complimentary tools to traditional methods, such as EEG power spectral density and phase-amplitude couplings to examine the seizure formations at millimeter scales.

Overall, the summary of our findings is that phase slip rates and phase slip accelerations change significantly during prolonged non-motor seizure activity and possibly can be used as additional biomarkers to study the spatiotemporal behavior of seizures. These tools are generic and can also be used to analyze the EEG data during various conditions, such as resting state and during cognitive tasks.

CRediT authorship contribution statement

Ceon Ramon: Methodology, Software, Validation, Formal analysis, Writing – original draft, Visualization. **Alexander Doud:** Data curation, Software development, Validation, Writing – review & editing. **Mark D. Holmes:** Conceptualization, Writing – review & editing, Supervision, Project administration, Funding acquisition and Resources acquisition.

Declaration of competing interest

All authors declare that there is no conflict of interest.

Data availability

Microgrid seizure (μECoG) data is publicly available on the Open Science Framework web page (https://osf.io) which is operated by the Center for Open Science. Also, the same data is available from all authors.

Appendix A. Peer Review Overview and Supplementary data

A Peer Review Overview and (sometimes) Supplementary data associated with this article can be found, in the online version, at https://doi.org/10.1016/j.crneur.2024.100126.

References

Beggs, J.M., Timme, N., 2012. Being critical of criticality in the brain. Front. Physiol. 3, 163. https://doi.org/10.3389/fphys.2012.00163.

Bhattacharya, B.S., Coyle, D., Maguire, L.P., 2011. A thalamo-cortico-thalamic neural mass model to study alpha rhythms in Alzheimer's disease. Neural Network. : the official journal of the International Neural Network Society 24 (6), 631–645. https://doi.org/10.1016/j.neunet.2011.02.009.

Brandenburg, M.A., 2019. Prescription opioids are associated with population mortality in US deep south middle-age non-hispanic whites: an ecological time series study. Front. Public Health 7, 252. https://doi.org/10.3389/fpubh.2019.00252.

Budd, J.M.L., Kisvárday, Z.F., 2012. Communication and wiring in the cortical connectome. Front. Neuroanat. 6, 42. https://doi.org/10.3389/fnana.2012.00042.

Capolupo, A., Freeman, W.J., Vitiello, G., 2013. Dissipation of 'dark energy' by cortex in knowledge retrieval. Phys. Life Rev. 10 (1), 85–94. https://doi.org/10.1016/j.plrev.2013.01.001.

Freeman, W.J., Barrie, J.M., 2000. Analysis of spatial patterns of phase in neocortical gamma EEGs in rabbit. J. Neurophysiol. 84 (3), 1266–1278. https://doi.org/10.1152/jn.2000.84.3.1266.

Freeman, W.J., Quiroga, R.Q., 2013. Basic concepts for spatial analysis. In: Freeman, W. J., Quiroga, R.Q. (Eds.), Imaging Brain Function with EEG: Advanced Temporal and Spatial Analysis of Electroencephalographic Signals. Springer, New York, NY, pp. 87–123. https://doi.org/10.1007/978-1-4614-4984-3_6.

Freeman, W.J., Vitiello, G., 2006. Nonlinear brain dynamics as macroscopic manifestation of underlying many-body dynamics. Phys. Life Rev. 3 (2), 93–118. https://doi.org/10.1016/j.plrev.2006.02.001.

Freeman, W.J., Burke, B.C., Holmes, M.D., 2003. Aperiodic phase re-setting in scalp EEG of beta-gamma oscillations by state transitions at alpha-theta rates. Hum. Brain Mapp. 19 (4), 248–272. https://doi.org/10.1002/hbm.10120.

Freeman, W.J., Holmes, M.D., West, G.A., Vanhatalo, S., 2006a. Dynamics of human neocortex that optimizes its stability and flexibility. Int. J. Intell. Syst. 21, 881–901. https://doi.org/10.1002/int.20167.

Freeman, W.J., Holmes, M.D., West, G.A., Vanhatalo, S., 2006b. Fine spatiotemporal structure of phase in human intracranial EEG. Clin. Neurophysiol. 117, 1228–1243. https://doi.org/10.1016/j.clinph.2006.03.012.

Hashimoto, H., Khoo, H.M., Yanagisawa, T., Tani, N., Oshino, S., Kishima, H., Hirata, M., 2021. Phase-amplitude coupling of ripple activities during seizure evolution with theta phase. Clin. Neurophysiol. 132, 1243–1253. https://doi.org/10.1016/j.clinph.2021.03.007.

Hashimoto, H., Khoo, H.M., Yanagisawa, T., Tani, N., Oshino, S., Hirata, M., Kishima, H., 2022. Frequency band coupling with high-frequency activities in tonic-clonic seizures shifts from θ to δ band. Clin. Neurophysiol. 137, 122–131. https://doi.org/10.1016/j.clinph.2022.02.015.

Hyndman, R.J., Athanasopoulos, G., 2018. Forecasting: Principles and Practice, 2nd edition, Ch 8. OTexts: Melbourne, Australia. OTexts.com/fp.2. (Accessed 30 January 2022).

Jansen, B.H., Rit, V.G., 1995. Electroencephalogram and visual evoked potential generation in a mathematical model of coupled cortical columns. Biol. Cybern. 73 (4), 357–366. https://doi.org/10.1007/BF00199471.

Jirsa, V., Wang, H., Triebkorn, P., Hashemi, M., Jha, J., Gonzalez-Martinez, J., Guye, M., Makhalova, J., Bartolomei, F., 2023. Personalised virtual brain models in epilepsy. The Lancet. Neurology 22 (5), 443–454. https://doi.org/10.1016/S1474-4422(23)00008-X.

Kantzeli, A., Brandt, C., Tomka-Hoffmeister, M., Woermann, F., Bien, C.G., 2021. De novo aphasic status epilepticus: finally making the diagnosis by long-term EEG. Epilepsy & behavior reports 17, 100513. https://doi.org/10.1016/j.ebr.2021.100513.

Kleen, J.K., Chung, J.E., Sellers, K.K., Zhou, J., Triplett, M., Lee, K., Tooker, A., Haque, R., Chang, E.F., 2021. Bidirectional propagation of low frequency oscillations over the human hippocampal surface. Nat. Commun. 12 (1), 2764. https://doi.org/10.1038/s41467-021-22850-5.

Kim, Y., Alimperti, S., Choi, P., Noh, M., 2022. An inkjet printed flexible electrocorticography (ECoG) microelectrode array on a thin parylene-C film. Sensors 22 (3), 1277. https://doi.org/10.3390/s22031277.

Kozma, R., Freeman, W.J., 2017. Cinematic operation of the cerebral cortex interpreted via critical transitions in self-organized dynamic systems. Front. Syst. Neurosci. 11, 10. https://doi.org/10.3389/fnsys.2017.00010.

Kuo, C., Blakely, T.M., Wander, J.D., Sarma, D., Wu, J., Casimo, K., Weaver, K.E., Ojemann, J.G., 2019. Context-dependent relationship in high-resolution micro-ECoG studies during finger movements. J. Neurosurg. 32 (5), 1358–1366. https://doi.org/10.3171/2019.1.JNS181840.

Kuo, C.H., Tu, T.H., Chen, K.T., 2023. Editorial: advanced technological applications in neurosurgery. Frontiers in surgery 10, 1277997. https://doi.org/10.3389/fsurg.2023.1277997.

Lara-Benítez, P., Carranza-García, M., Riquelme, J.C., 2021. An experimental review on deep learning architectures for time series forecasting. Int. J. Neural Syst. 31 (3), 2130001 https://doi.org/10.1142/S0129065721300011.

Meijs, J.W., Weier, O.W., Peters, M.J., van Oosterom, A., 1989. On the numerical accuracy of the boundary element method. IEEE Trans. Biomed. Eng. 36, 1038–1049. https://doi.org/10.1109/10.40805.

Myers, M.H., Kozma, R., Davis, J.J., Ilin, R., 2014. Phase cone detection optimization in EEG data. In: Proceedings of the 2014 International Joint Conference on Neural Networks (IJCNN). IEEE), Piscataway, NJ, pp. 2504–2511. https://doi.org/10.1109/IJCNN.2014.6889880.

Panagiotides, H., Freeman, W.J., Holmes, M.D., Pantazis, D., 2011. Behavioral states may be associated with distinct spatial patterns in electrocorticogram. Cogn Neurodyn 5 (1), 55–66. https://doi.org/10.1007/s11571-010-9139-4.

Pikovsky, A., Rosenblum, M., Kurths, J., 2001. Synchronization: a Universal Concept in Non-linear Sciences. Cambridge University Press, Cambridge UK.

Pinotsis, D.A., Moran, R.J., Friston, K.J., 2012. Dynamic causal modeling with neural fields. Neuroimage 59 (2), 1261–1274. https://doi.org/10.1016/j.neuroimage.2011.08.020.

Pizarro, R., Richner, T., Brodnick, S., Thongpang, S., Williams, J., Van Veen, B., 2017. Estimating cortical column sensory networks in rodents from micro-electrocorticograph (μECoG) recordings. Neuroimage 163, 342–357. https://doi.org/10.1016/j.neuroimage.2017.09.043.

Ramon, C., Freeman, W.J., Holmes, M., Ishimaru, A., Haueisen, J., Schimpf, P.H., Rezvanian, E., 2009. Similarities between simulated spatial spectra of scalp EEG, MEG and structural MRI. Brain Topogr. 22 (3), 191–196. https://doi.org/10.1007/s10548-009-0104-7.

Ramon, C., Garguilo, P., Fridgeirsson, E.A., Haueisen, J., 2014. Changes in scalp potentials and spatial smoothing effects of inclusion of dura layer in human head models for EEG simulations. Front. Neuroeng. 7, 32. https://doi.org/10.3389/fneng.2014.00032.

Ramon, C., Holmes, M.D., 2015. Spatiotemporal phase clusters and phase synchronization patterns derived from high density EEG and ECoG recordings. Curr. Opin. Neurobiol. 31, 127–132. https://doi.org/10.1016/j.conb.2014.10.001.

Ramon, C., Holmes, M.D., 2020. Increased phase cone turnover in 80–250 Hz bands occurs in the epileptogenic zone during interictal periods. Front. Hum. Neurosci. 14, 615744 https://doi.org/10.3389/fnhum.2020.615744.

Ramon, C., Holmes, M.D., Freeman, W.J., 2013. Increased phase clustering in epileptogenic areas measured with 256-channel dense array EEG. J. Neurol. Transl. Neurosci. 2, 1029.

Ramon, C., Holmes, M.D., Wise, M.V., Tucker, D., Jenson, K., Kinn, S.R., 2018. Oscillatory patterns of phase cone formations near to epileptic spikes derived from 256-channel scalp EEG data. Comput. Math. Methods Med. 2018, 9034543 https://doi.org/10.1155/2018/9034543.

Ramon, C., Graichen, U., Gargiulo, P., Zanow, F., Knösche, T.R., Haueisen, J., 2023. Spatiotemporal phase slip patterns for visual evoked potentials, covert object naming tasks, and insight moments extracted from 256 channel EEG recordings. Front. Integr. Neurosci. 17, 1087976 https://doi.org/10.3389/fnint.2023.1087976.

Ravishankar, N., 1994. Relative curvature measures of nonlinearity for time series models. Commun. Stat. Simulat. Comput. 23 (2), 415–430. https://doi.org/10.1080/03610919408813178.

Ruiz, Y., Pockett, S., Freeman, W.J., Gonzalez, E., Li, G., 2010. A method to study global spatial patterns related to sensory perception in scalp EEG. J. Neurosci. Methods 191, 110–118. https://doi.org/10.1016/j.jneumeth.2010.05.021.

Schimpf, P., Ramon, C., Haueisen, J., 2002. Dipoles models for the EEG and MEG. IEEE Trans. Biomed. Eng. 49, 409–418. https://doi.org/10.1109/10.995679.

Seymour, J.P., Wu, F., Wise, K.D., Yoon, E., 2017. State-of-the-art MEMS and microsystem tools for brain research. Microsystems & nanoengineering 3, 16066. https://doi.org/10.1038/micronano.2016.66.

Shokoueinejad, M., Park, D.W., Jung, Y.H., Brodnick, S.K., Novello, J., Dingle, A., Swanson, K.I., Baek, D.H., Suminski, A.J., Lake, W.B., Ma, Z., Williams, J., 2019. Progress in the field of micro-electrocorticography. Micromachines 10 (1), 62. https://doi.org/10.3390/mi10010062.

Stead, M., Bower, M., Brinkmann, B.H., Lee, K., Marsh, W.R., Meyer, F.B., Litt, B., Van Gompel, J., Worrell, G.A., 2010. Microseizures and the spatiotemporal scales of human partial epilepsy. Brain : J. Neurol. 133 (9), 2789–2797. https://doi.org/10.1093/brain/awq190.

Sun, J., Barth, K., Qiao, S., Chiang, C.H., Wang, C., Rahimpour, S., Trumpis, M., Duraivel, S., Dubey, A., Wingel, K.E., Rachinskiy, I., Voinas, A.E., Ferrentino, B., Southwell, D.G., Haglund, M.M., Friedman, A.H., Lad, S.P., Doyle, W.K., Solzbacher, F., Cogan, G., et al., 2022. Intraoperative microseizure detection using a high-density micro-electrocorticography electrode array. Brain communications 4 (3), fcac122. https://doi.org/10.1093/braincomms/fcac122.

Swadlow, H.A., Waxman, S.G., 2012. Axonal conduction delays. Scholarpedia 7, 1451. https://doi:10.4249/scholarpedia.1451.

Thatcher, R.W., North, D.M., Biver, C.J., 2009. Self-organized criticality and the development of EEG phase reset. Hum. Brain Mapp. 30 (2), 553–574. https://doi.org/10.1002/hbm.20524.

Thatcher, R.W., North, D.M., Biver, C.J., 2014. LORETA EEG phase reset of the default mode network. Front. Hum. Neurosci. 8, 529. https://doi.org/10.3389/fnhum.2014.00529.

Toker, D., Pappas, I., Lendner, J.D., Frohlich, J., Mateos, D.M., Muthukumaraswamy, S., Carhart-Harris, R., Paff, M., Vespa, P.M., Monti, M.M., Sommer, F.T., Knight, R.T., D'Esposito, M., 2022. Consciousness is supported by near-critical slow cortical electrodynamics. Proc. Natl. Acad. Sci. U.S.A. 119 (7), e2024455119 https://doi.org/10.1073/pnas.2024455119.

Wang, S.H., Siebenhühner, F., Arnulfo, G., Myrov, V., Nobili, L., Breakspear, M., Palva, S., Palva, J.M., 2023. Critical-like brain dynamics in a continuum from second- to first-order phase transition. J. Neurosci. : the official journal of the Society

for Neuroscience 43 (45), 7642–7656. https://doi.org/10.1523/JNEUROSCI.1889-22.2023.

Wang, X., Gkogkidis, C.A., Iljina, O., Fiederer, L.D.J., Henle, C., Mader, I., Kaminsky, J., Stieglitz, T., Gierthmuehlen, M., Ball, T., 2017. Mapping the fine structure of cortical activity with different micro-ECoG electrode array geometries. J. Neural. Eng. 14 (5), 056004 https://doi.org/10.1088/1741-2552/aa785e.

Wu, Q., Zhao, C.W., Long, Z., Xiao, B., Feng, L., 2018. Anatomy based networks and topology alteration in seizure-related cognitive outcomes. Front. Neuroanat. 12, 25. https://doi.org/10.3389/fnana.2018.00025.

Yasugi, D., Sasaki, T., Taniguchi, G., 2018. Periodic slow waves presenting as ictal electroencephalography findings in complex partial status epilepticus. Case Rep. Neurol. 10 (2), 199–206. https://doi.org/10.1159/000490939.